PHYSICAL REVIEW LETTERS

Systematics of Proton Emission

D. S. Delion

National Institute of Physics and Nuclear Engineering, POB MG-6, Bucharest-Măgurele, Romania

R. J. Liotta and R. Wyss

KTH, Alba Nova University Center, SE-10691 Stockholm, Sweden
(Received 2 September 2005; published 22 February 2006)

A very simple formula is presented that relates the logarithm of the half-life, corrected by the centrifugal barrier, with the Coulomb parameter in proton decay processes. The corresponding experimental data lie on two straight lines which appear as a result of a sudden change in the nuclear shape marking two regions of deformation independently of the angular momentum of the outgoing proton. This feature provides a powerful tool to assign experimentally quantum numbers in proton emitters.

Nearly a century ago one of the most challenging problems in physics was the understanding of the Geiger-Nuttall rule, which says that the logarithm of the half-life in α decay is inverse proportional to the energy of the outgoing α particle, i.e., its Q value. It can be asserted that the probabilistic interpretation of quantum mechanics started by the explanation given by Gamow to that rule as a consequence of the quantum penetration of the α particle through the Coulomb barrier [1]. Nowadays the challenge in nuclear physics is related to rare nuclei, i.e., nuclei lying very far from the stability line which decay rapidly by particle emission (neutron and proton drip lines) [2]. The exploration of the drip lines is one of the ambitions of the projected radioactive nuclear beam facilities as, e.g., the Rare Isotope Accelerator (RIA) [3].

By plotting the logarithm of the half-lives as a function of Q_p, i.e., the kinetic energy of the emitted proton, one does not obtain a clear graphical pattern of the experimental data, as for the Geiger-Nuttall rule. As seen in Fig. 1(a) [4], such a plot does not reveal any obvious trend. The reason for this disorder is that not only Q_p but also the height and width of the Coulomb and centrifugal barriers, in which the proton is trapped before decaying, determine the decay width. The role of the centrifugal barrier in proton emission is more important than in α decay due to the smaller proton reduced mass and also because in most cases the proton carries a nonvanishing angular momentum. The half-life corresponding to the wave with given quantum numbers (l, j) can be written as [5]

$$T_{1/2} = \frac{\ln 2}{v} \left| \frac{H_l^{(+)}(\chi, \rho)}{s_{lj}(R, \beta)} \right|^2, \tag{1}$$

where $H_l^{(+)}$ is the Coulomb-Hankel spherical wave, $\chi = 2(Z - 1)e^2/(\hbar v)$ is the Coulomb parameter (which determines the Coulomb barrier), Z is the charge number of the mother nucleus, $v = \hbar k/\mu = \sqrt{2Q_p/\mu}$ is the velocity of the outgoing proton, μ is the reduced mass of the proton-

daughter system, $\rho = kR$, and the spectroscopic function is given by [6]

$$s_{lj}(R, \beta) = \sum_{l'j'} K_{lj;l'j'}(R, \beta) s_{l'j'}^{(0)} f_{l'j'}(R, \beta), \tag{2}$$

where $s_{lj}^{(0)}$ is the so-called spectroscopic factor (the particle amplitude u_{lj} within the super fluid model) and f_{lj} are the components of the internal wave function (the standard Nilsson function within the adiabatic approach). We mention here that $|s_{lj}^{(0)}|^2 \approx 0.5$. Moreover, for spherical emitters a clear dependence of the spectroscopic factor upon the
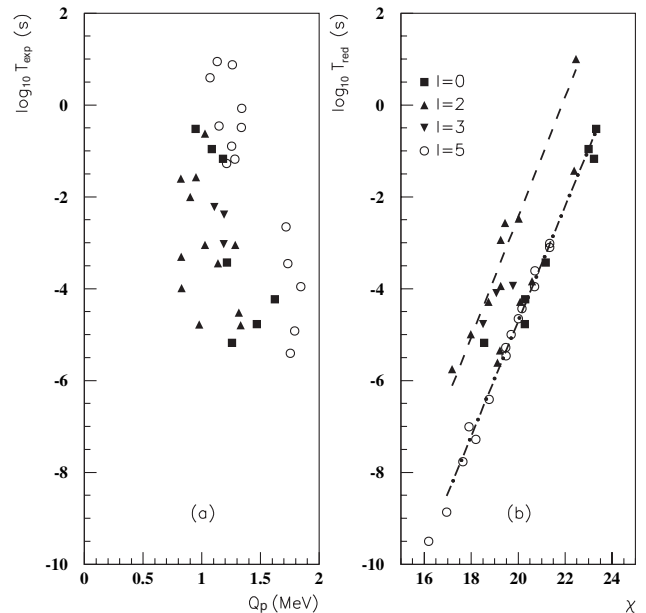

FIG. 1. (a) Logarithm of the experimental half-lives corresponding to proton decay as a function of the Q value. The data are taken from Ref. [4]. (b) Values of $\log_{10} T_{\text{red}}$, Eq. (6), as a function of the Coulomb parameter χ. The numbers labeling the different symbols correspond to the l values of the outgoing proton. The two lines are computed according to Eq. (8).

shell occupancy was in evidence [7]. The asymptotic propagator matrix is given by

$$K_{lj;l'j'}(R, \beta) \equiv H_l^{(+)}(\chi, \rho)[\mathcal{H}^{(+)}(R, \beta)]_{lj;l'j'}^{-1}$$
$$= \delta_{ll'}\delta_{jj'} + \Delta K_{lj;l'j'}(R, \beta). \quad (3)$$

Here $\mathcal{H}_{lj;l'j'}^{(+)}(R, \beta)$ is the matrix of solutions with an outgoing boundary behavior, i.e., $\mathcal{H}_{lj;l'j'}^{(+)}(R, \beta) \rightarrow_{R\to\infty} \delta_{ll'} \times \delta_{jj'}H_l^{(+)}(\chi, \rho)$. Thus, the relation (1) has the same form as in the spherical case, but for deformed systems the spectroscopic function is a superposition of the different channel components f_{lj}.

The ratio $H_l^{(+)}/s_{lj}$, entering Eq. (1) [which is just the inverse of the scattering amplitude in the (l, j) channel] does not depend upon the radius and this is an important test of accuracy in any coupled channels scheme. A good approximation of the function $H_l^{(+)}$ for physical situations is given by the WKB value, i.e., [5]

$$H_l^{(+)}(\chi, \rho) \approx G_l(\chi, \rho)$$
$$\approx C_l(\chi, \rho)(\cot\alpha)^{1/2} \exp[\chi(\alpha - \sin\alpha\cos\alpha)], \quad (4)$$

where G_l is the irregular Coulomb function. The influence of the centrifugal barrier is fully contained in the function C_l, which is given by

$$C_l(\chi, \rho) = \exp\left[\frac{l(l + 1)}{\chi}\tan\alpha\right],$$
$$\cos^2\alpha = \frac{Q_p}{V_c(R)} = \frac{\rho}{\chi}, \quad (5)$$

$V_c(R)$ is the Coulomb potential at distance R. We will choose this distance as the matching radius, for which we will adopt the standard form, i.e., $R = 1.2(A_d^{1/3} + A_p^{1/3})$, where A_d is the mass number of the daughter nucleus and $A_p = 1$. The dependence of the centrifugal factor upon the distance, entering through α, is very weak around that value of R. Defining a reduced half-life as

$$T_{\text{red}} = \frac{T_{1/2}}{C_l^2} = \frac{F(\chi, \rho)}{|s_{lj}(R, \beta)|^2}, \quad (6)$$

where

$$F(\chi, \rho) = \frac{\ln 2}{v}\cot\alpha\exp[2\chi(\alpha - \sin\alpha\cos\alpha)], \quad (7)$$

one sees that T_{red} should not depend upon the angular momentum l if plotted against the dimensionless Coulomb parameter χ. Moreover, $\log_{10}T_{\text{red}}$ is a linear function of χ independent of the value of l, provided the velocity v, the function s_{lj}, and the parameter α, which depend upon the Q value, has a smooth behavior in this logarithmic scale. Notice that the value of T_{red} is model independent since the only theoretical quantity entering in

its definition is the function C_l^2, which is a by-product of the barrier penetration process. But it is important to stress that this entire analysis is based upon the assumption that the proper value of l, that is, the one that determines the experimental half-life $T_{1/2}$, is used. Otherwise, and since $T_{1/2}$ is strongly l dependent, that straight line pattern would be completely spoiled.

To check the rather straightforward conclusions reached above we evaluated $\log_{10}T_{\text{red}}$ in cases where experimental data are available, as shown in Table I. We considered proton emitters with $Z > 50$ and angular momentum as given in Ref. [4]. The orbital and total angular momenta of the proton in the mother nucleus labeling a given partial wave will be denoted by (l_m, j_m). The corresponding outgoing values (at large distances) will be (l, j). Angular momentum conservation requires that $\vec{J}_m = \vec{J}_d + \vec{j}$, where J_m (J_d) is the angular momentum of the mother (daughter) nucleus. In the case of odd decaying nuclei to the ground state with $J_d = 0$, it follows that $J_m = j_m$. If, in addition, the nucleus is spherical then $j_m = j$ and $l_m = l$, where l_m is the orbital angular momentum of the single quasiproton state in the mother nucleus. The value of j_m in Table I is the angular momentum of the proton outside the nucleus. It is often extracted from theoretical predictions.

With the values of l, χ, and $\log_{10}T_{\text{red}}$ of Table I we produced the plot shown in Fig. 1(b). Amazingly enough, the points lie all approximately along two straight lines. The nuclei on the upper line correspond to the first 12 cases in Table I, i.e., those with $Z < 68$. It is important to point out that the angular momenta in all cases of Fig. 1(b) are as reported in the literature, except the nucleus ^{109}I for which we changed the angular momentum $l = 0$ of Ref. [4] to $l = 2$. We did this because we performed a coupled channels calculation showing a larger component with $l = 2$ (0.37) in comparison with $l = 0$ (0.02) for the $1/2+$ deformed state at the Fermi level. Note that this assignment is also in agreement with the systematics in heavier isotopes, like, e.g., in ^{111}I [11].

Using a fitting procedure we found that the experimental half-lives can be reproduced by the formula

$$\log_{10}T_{\text{red}}^{(k)} = a_k(\chi - 20) + b_k,$$
$$a_1 = 1.31, \qquad b_1 = -2.44 \quad \text{for } Z < 68$$
$$\text{and} \quad a_2 = 1.25, \qquad b_2 = -4.71 \quad \text{for } Z > 68, \quad (8)$$

where $k = 1$ corresponds to the upper line in Fig. 1(b). The standard errors are $\sigma_1 = 0.26$ and $\sigma_2 = 0.23$, corresponding to a mean factor less than two.

These two straight lines may have been induced either by an abrupt change in the Q values or in the structure of the different emitters, or by both. The Q-value dependence affects only the function $F(\chi, \rho)$. We therefore plotted this function against χ in Fig. 2. One sees in this figure the same pattern as in Fig. 1(b); namely, there appear two lines, but now the upper line includes only six emitters with $Z < 68$.

TABLE I.   Data used in the calculation. The spin of the proton moving inside the mother nucleus (j_m), the proton Q value (Q_p), and the emitter half-life (T_{exp}) are from Refs. [4,8,9]. The quadrupole deformation parameters β are from Ref. [10] and the quantities l, χ, α, T_{red}, and s_{lj} are as explained in the text. All half-lives are in seconds. Stars in the emitters indicate excited states.

No.	Emitter	l	j_m^π	Q_p (keV)	χ	β	α	$\log_{10}T_{exp}$	$\log_{10}T_{red}$	$\log_{10}s_{lj}^{-2}$
1	$^{105}_{51}$Sb	2	$5/2^+$	491(15)	22.457	0.081	1.353	2.049	1.000	1.525
2	$^{109}_{53}$I	2	$3/2^+$	829(3)	17.977	0.160	1.290	−3.987	−4.994	1.810
3	$^{112}_{55}$Cs	2	$3/2^+$	824(7)	18.728	0.208	1.296	−3.301	−4.287	1.701
4	$^{113}_{55}$Cs	2	$3/2^+$	978(3)	17.171	0.207	1.270	−4.777	−5.747	1.213
5	$^{117}_{57}$La	2	$3/2^+$	823(5)	19.437	0.290	7.052	−1.602	−2.565	2.680
6	$^{121}_{59}$Pr	2	$3/2^+$	900(10)	19.253	0.318	7.119	−2.000	−2.939	2.756
7	$^{130}_{63}$Eu	2	$3/2^+$	1028(15)	19.263	0.331	7.263	−3.046	−3.941	2.146
8	$^{131}_{63}$Eu	2	$3/2^+$	951(7)	20.028	0.331	1.289	−1.575	−2.473	2.592
9	$^{135}_{65}$Tb	3	$7/2^-$	1188(7)	18.499	0.325	7.341	−3.027	−4.770	2.548
10	$^{140}_{67}$Ho	3	$7/2^-$	1106(10)	19.775	0.297	7.416	−2.222	−3.937	1.864
11	$^{141}_{67}$Ho	3	$7/2^-$	1190(8)	19.064	0.286	1.261	−2.387	−4.094	2.672
12	$^{141}_{67}$Ho*	0	$1/2^+$	1256(8)	18.557	0.286	1.252	−5.180	−5.180	2.268
13	$^{145}_{69}$Tm	5	$11/2^-$	1753(10)	16.185	−0.199	7.490	−5.409	−9.500	1.307
14	$^{146}_{69}$Tm	5	$11/2^-$	1210(5)	19.481	−0.199	1.261	−1.276	−5.460	0.943
15	$^{146}_{69}$Tm*	5	$11/2^-$	1148(5)	20.001	−0.199	1.270	−0.456	−4.651	1.053
16	$^{147}_{69}$Tm	5	$11/2^-$	1071(3)	20.708	−0.190	1.280	0.591	−3.613	1.148
17	$^{147}_{69}$Tm*	2	$3/2^+$	1139(5)	20.080	−0.190	1.271	−3.444	−4.282	1.324
18	$^{150}_{71}$Lu	5	$11/2^-$	1283(4)	19.477	−0.164	1.255	−1.180	−5.280	1.314
19	$^{150}_{71}$Lu*	2	$3/2^+$	1317(15)	19.224	−0.164	1.251	−4.523	−5.342	1.592
20	$^{151}_{71}$Lu	5	$11/2^-$	1255(3)	19.694	−0.156	1.259	−0.896	−4.996	1.316
21	$^{151}_{71}$Lu*	2	$3/2^+$	1332(10)	19.116	−0.156	1.249	−4.796	−5.613	1.475
22	$^{155}_{73}$Ta	5	$11/2^-$	1791(10)	16.958	0.008	1.199	−4.291	−8.864	1.293
23	$^{156}_{73}$Ta	2	$3/2^+$	1028(5)	22.384	−0.050	1.292	−0.620	−1.433	1.448
24	$^{156}_{73}$Ta*	5	$11/2^-$	1130(8)	21.350	−0.050	1.278	0.949	−3.099	1.177
25	$^{157}_{73}$Ta	0	$1/2^+$	947(7)	23.322	0.045	1.303	−0.523	−0.523	1.099
26	$^{160}_{75}$Re	2	$3/2^+$	1284(6)	20.587	0.080	1.261	−3.046	−3.837	1.649
27	$^{161}_{75}$Re	0	$1/2^+$	1214(6)	21.172	0.080	1.270	−3.432	−3.432	1.275
28	$^{161}_{75}$Re*	5	$11/2^-$	1338(6)	20.167	0.080	1.254	−0.488	−4.433	1.626
29	$^{164}_{77}$Ir	5	$11/2^-$	1844(9)	17.644	0.089	1.201	−3.959	−7.768	1.838
30	$^{165}_{77}$Ir	5	$11/2^-$	1733(7)	18.201	0.099	1.212	−3.456	−7.279	1.594
31	$^{166}_{77}$Ir*	5	$11/2^-$	1340(8)	20.699	0.107	1.257	−0.076	−3.955	1.578
32	$^{167}_{77}$Ir	0	$1/2^+$	1086(6)	22.993	0.116	1.289	−0.959	−0.959	1.492
33	$^{167}_{77}$Ir*	5	$11/2^-$	1261(7)	21.338	0.116	1.266	0.875	−3.012	1.670
34	$^{171}_{79}$Au	0	$1/2^+$	1469(17)	20.291	−0.105	1.245	−4.770	−4.770	1.498
35	$^{171}_{79}$Au*	5	$11/2^-$	1718(6)	18.763	−0.105	1.217	−2.654	−6.414	1.901
36	$^{177}_{81}$Tl	0	$1/2^+$	1180(20)	23.223	−0.050	1.282	−1.174	−1.174	1.342
37	$^{177}_{81}$Tl*	5	$11/2^-$	1986(10)	17.901	−0.053	1.192	−3.347	−7.006	2.648
38	$^{185}_{83}$Bi	0	$1/2^+$	1624(16)	20.293	−0.052	1.232	−4.229	−4.229	2.436

In fact, the deviations from the two lines in Fig. 2 are much larger here than in Fig. 1(b), corresponding to an error of about 1 order of magnitude. This forces us to conclude that, although the pattern shown in Fig. 2 corresponding to $s_{lj}(\beta) = $ const is similar to the dependence between ρ and χ, this effect cannot be the only reason behind the two straight lines of Fig. 1(b). The only other source that may contribute to that alignment is an abrupt change in the nuclear structure of the emitters. We therefore correlated the deformation values calculated in Ref. [10] with the
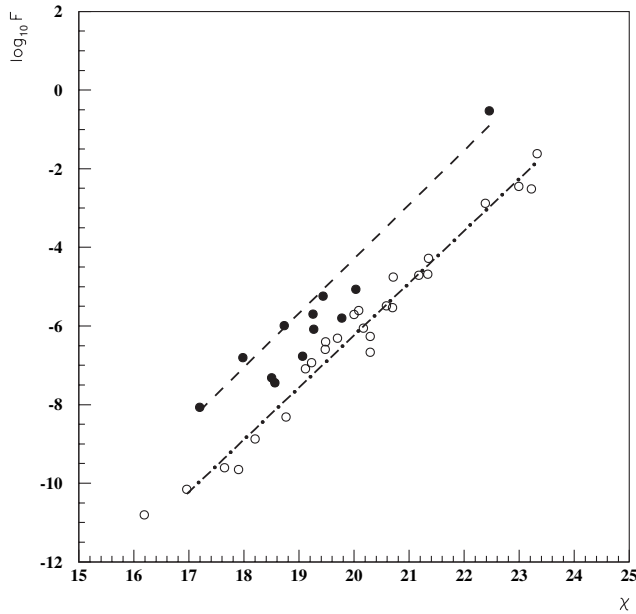
FIG. 2.   The logarithm of $F(\chi, \rho)$ (s/fm), Eq. (7), as a function of χ. The two straight lines are average values to guide the eye. Filled symbols correspond to the first 12 cases of Table I.

FIG. 3.   (a) Dependence of the quadrupole deformation parameter β, as given in Table I, upon the charge number Z. Filled symbols correspond to the first 12 cases of Table I. Notice that β is the same in this scale for the isotopes Cs and also for the two states in Ho. (b) The logarithm of the spectroscopic function s_{lj}^{-2}, defined by Eq. (1) and given in the last column of the Table I, versus the charge number Z.

determined half-lives. In Fig. 3(a) we show the deformation parameter β as a function of Z. At the proton drip line between $Z = 67$ and $Z = 69$ a pronounced change occurs, from a large prolate shape with $\beta \approx 0.3$ to an oblate shape with $\beta \approx -0.2$. These shapes are substantiated by measurements of moments of inertia. In order to analyze the dependence of the half-life upon the internal structure of the nucleus we plot in Fig. 3(b) the quantity $\log_{10} s_{lj}^{-2}$ as a function of the charge number Z. It is worthwhile to emphasize once again that this is a model independent function.

One remarks a striking correlation between Figs. 3(a) and 3(b). After the jump occurring at $Z = 68$, where an abrupt shape change occurs, the deformation of the nuclei lying on the lower line smoothly increases. One can then assert that these lines reflect two regions of nuclei separated by a sharp transition between the prolate and oblate regimes.

There are two points in Fig. 1(b) that deviate conspicuously from the upper straight line. They correspond to ^{140}Ho ($l = 3$) and ^{141}Ho* ($l = 0$). In Fig. 3(a) one sees that these nuclei are situated at the border between the two regions of deformation.

In conclusion, we have presented in this Letter a simple formula for proton decay [Eq. (8)] similar to the Geiger-Nuttall rule. This formula enables the precise assignment of spin and parity for proton decaying states. The only quantities that are needed are the half-life of the mother nucleus and the proton Q value. As a function of these quantities, corrected by the centrifugal barrier [Eq. (6)], the experimental data of proton emitters with $Z > 50$ lie along
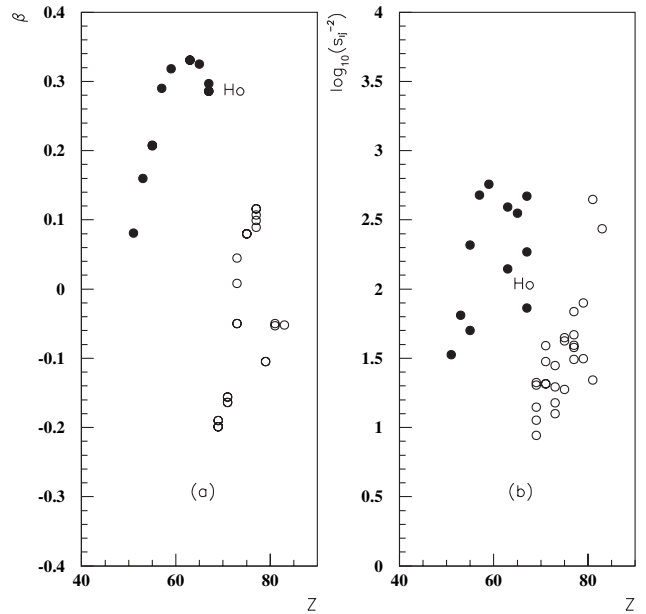
two straight lines. Taking into account that ^{140}Ho ^{141}Ho* are the only emitters that deviate from the systematics, one concludes the remarkable fact: proton emitters with $Z > 50$ follow simple systematics, which are obviously correlated with two regions of quadrupole deformation, as can be seen by plotting $\log_{10} s^{-2}$ versus β.

[1] G. Gamow, Z. Phys. **51**, 204 (1928).
[2] P. J. Woods and C. N. Davids, Annu. Rev. Nucl. Part. Sci. **47**, 541 (1997).
[3] Rare isotope accelerator. Argonne web p., www.anl.gov/ria, and Rare isotope accelerator (RIA). NSCL web p., www.nscl.msu.edu/ria.
[4] A. A. Sonzogni, Nuclear Data Sheets **95**, 1 (2002).
[5] P. O. Fröman, K. Dan. Vidensk. Selsk. Mat. Fys. Medd. **1** (1957).
[6] D. S. Delion, R. J. Liotta, and R. Wyss, Phys. Rep. **424**, 113 (2006).
[7] S. Åberg, P. B. Semmes, and W. Nazarewicz, Phys. Rev. C **56**, 1762 (1997).
[8] P. J. Woods et al., Phys. Rev. C **69**, 051302(R) (2004).
[9] A. P. Robinson et al., Phys. Rev. Lett. **95**, 032502 (2005).
[10] P. Möller, R. J. Nix, W. D. Myers, and W. Swiatecki, At. Data Nucl. Data Tables **59**, 185 (1995).
[11] E. S. Paul et al., Phys. Rev. C **61**, 064320 (2000).